Annals of Nuclear Energy 36 (2009) 393–398

Contents lists available at ScienceDirect

Annals of Nuclear Energy

journal homepage: www.elsevier.com/locate/anucene

Monte Carlo study of photoneutron production in U-235 following perturbations in cross section data

S.D. Clarke *, S.A. Pozzi, M. Flaska, T.J. Downar

Department of Nuclear Engineering and Radiological Sciences, University of Michigan, Ann Arbor, MI 48109-2104, USA

ARTICLE INFO

Article history:
Received 8 October 2008
Received in revised form 19 November 2008
Accepted 19 November 2008
Available online 12 January 2009

ABSTRACT

Active photon interrogation systems may be employed to detect high-Z isotopes without significant spontaneous fission emissions. These systems induce photonuclear reactions with emissions (such as fission neutrons) that may be detected. However, there are inconsistencies in the literature reporting resonance photonuclear interaction data for many isotopes. Recent publications show variations as large as 20% between various measurements of photonuclear cross section data. A perturbation methodology utilizing the modular nature of the MCNPX/MCNP-PoliMi code system has been implemented and is applied here to highly-enriched uranium. Monoenergetic photon sources between 8 and 18 MeV were simulated; neutron detection was performed using the MCNP-PoliMi liquid scintillator model. At photon energies less than 12 MeV, the number of detected neutrons is approximately 70% sensitive to changes in the (γ,f) cross section and 30% sensitive to changes in the (γ,n) cross section. As gamma-ray energy increases the (γ,f) sensitivity increases and the (γ,n) sensitivity decreases. There is a small $(\gamma,2n)$ sensitivity at photon energies between 15 and 17 MeV. The ability of modern simulation tools to predict photonuclear responses is greatly limited in this energy region due to the high sensitivity of the simulated results to observed discrepancies in photonuclear cross section data.

1. Introduction

The detection of concealed fissile material is a difficult problem which is magnified for isotopes – such as uranium – without significant spontaneous fission emissions. Active photon interrogation systems may be employed to detect such isotopes. These systems utilize high-energy bremsstrahlung photons to induce photonuclear reactions (including fission) in the material of interest. The material may then be characterized by detecting these emissions. The Monte Carlo method is the most widely applied approach to the design and analysis of such systems (Flaska et al., 2004). In particular, the MCNPX/MCNP-PoliMi code system has been developed to simulate all aspects of these systems, from the source electrons to the final correlated detector response.

The quality of the initial nuclear data has a direct impact on the quality of the simulated results and there are clear inconsistencies in the literature reporting photonuclear interaction data for many isotopes. In fact, recent publications show variations as large as 20% between various measurements of photonuclear cross section data for uranium isotopes (Dupont et al., 2007; Giacri-Mauborgne et al., 2006). The most recent release of photonuclear interaction data is the ENDF/B-VII library, which offers several improvements over its predecessors, but does not address the observed, sometimes quite significant discrepancy in the measured data. Fig. 1 shows the ENDF-B/VII ^{235}U cross section data. These data are lower over the entire resonance region than other measurements, except for those by Varmalov et al. (1999). In particular, these cross sections are lower than the otherwise widely-accepted measurements by Caldwell et al. (1980) by as much as 20%.

Previous work has explored the sensitivity of photoneutron production to perturbations in photonuclear cross section data for interrogation of a depleted uranium target (Clarke et al., 2008). The methodology is applied here to a highly-enriched uranium (HEU) target for a range of monoenergetic photon sources.

2. Description of techniques

The MCNPX/MCNP-PoliMi code system was used for this analysis to obtain the most accurate simulation of the detector response. In addition, its modular nature makes it ideal for implementing the perturbation technique described here. A photonuclear source file may be generated using a modified version of MCNPX and read by MCNP-PoliMi (Pozzi et al., 2007).

2.1. Description of MCNP-PoliMi

The standard MCNPX perturbation routines are not available for photonuclear reactions[1] (Pelowitz, 2005). Therefore, a new

* Corresponding author. Tel.: +1 734 615 7830; fax: +1 734 763 4540.
E-mail address: clarkesd@umich.edu (S.D. Clarke).

[1] The MCNPX perturbation routines could be extended to handle photonuclear cross sections. However, the method applied here presents a simpler solution.

0306-4549/$ - see front matter © 2008 Elsevier Ltd. All rights reserved.
doi:10.1016/j.anucene.2008.11.023

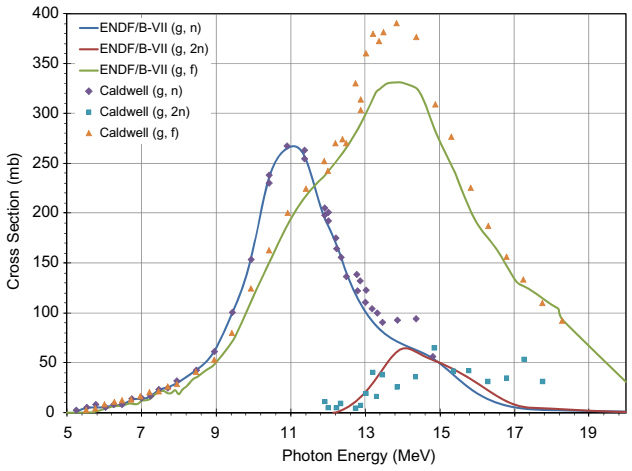

Fig. 1. Photonuclear reaction cross sections for ^{235}U from the ENDF/B-VII library. Measured data from Caldwell et al. (1980) are also shown.

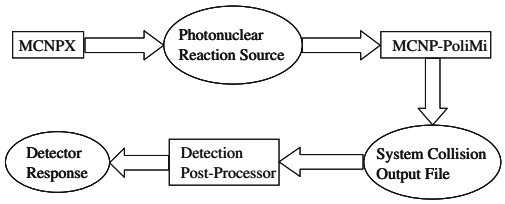

Fig. 2. Calculation flow of the MCNPX/MCNP-PoliMi code system.

methodology was developed and implemented that utilizes the modular nature of the MCNPX/MCNP-PoliMi code system (Clarke et al., 2008).

Fig. 2 illustrates the calculation flow of a typical MCNP-PoliMi simulation with a photonuclear source. A modified version of MCNPX transports the source photons to the target in analog mode. A "photonuclear reaction source file" is written that contains the energy of the interacting photon, the target isotope, the reaction type, and its geometric location.

The "reaction source file" is read by MCNP-PoliMi, which then transports the products of each source event through the system geometry. The energy released at each collision in the detectors, the corresponding time, the incident particle type, and the target nucleus are saved in a "collision output file". A post-processing code is then used to load the required data from this file and to compute the detector-specific response. Detector properties such as deadtime and detection threshold are chosen by the user.

2.2. Perturbation methodology

For any response that is directly proportional to the neutron flux – a detected time-of-flight (TOF) spectrum for example – linear superposition applies to all contributing responses. The total detector response to photonuclear emissions is therefore equal to the sum of the contributions from each photonuclear reaction

$$R = R_{(\gamma,n)} + R_{(\gamma,2n)} + \ldots + R_{(\gamma,xn)} + R_{(\gamma,f)}. \tag{1}$$

Each partial response is equal to the integral of the product of the neutron flux and the macroscopic photonuclear cross section times the detector response function operator

$$R_i = \int_{V,E,\Omega,E'\Omega'} D(\vec{r},E',\vec{\Omega}')v_i(E \rightarrow E',\vec{\Omega}\cdot\vec{\Omega}')\cdot\sum_i(\vec{r},E)\varphi(\vec{r},E,\vec{\Omega})\mathrm{d}V\mathrm{d}E\mathrm{d}\Omega\mathrm{d}E'\mathrm{d}\Omega'. \tag{2}$$

The cross section data are then perturbed in the following manner

$$\sum_i^*(\vec{r},E) = N(\vec{r})(1+\delta(E)_i)\sigma_i(\vec{r},E), \tag{3}$$

where N is the number density of the target material, $\delta(E)_i$ is the perturbation, and $\sigma_{i\sigma}$ is the microscopic interaction cross section. The perturbation may be applied as a function of photon energy. A point-wise approach will be applied here using a series of monoenergetic photons; a series of constant perturbations will be applied for each energy.

The photon flux in the target will also be slightly perturbed as a direct result of perturbing the *total* photon interaction cross section. However, the photonuclear cross section is a small contribution to the total photon interaction cross section (which consists primarily of photoatomic interactions). Consequently, it is valid to assume that the photon flux remains approximately constant following small perturbations to the photonuclear cross section data.

For a constant perturbation (i.e. the same cross section variation over all energies), and a constant photon flux, the perturbed response may be written as

$$R_i^* = (1+\delta_i)R_i. \tag{4}$$

In other words, the perturbed response is equal to the sum of each partial response multiplied by the corresponding perturbation. For the cases considered here the perturbed photonuclear response is equal to

$$R^* = (1+\delta_{(\gamma,n)})R_{(\gamma,n)} + (1+\delta_{(\gamma,2n)})R_{(\gamma,2n)} + (1+\delta_{(\gamma,f)})R_{(\gamma,f)}. \tag{5}$$

It is important to note that the total cross section will be modified as a result of these individual perturbations. In reality, the total cross sections is well known. Therefore, changes to a single cross section would be compensated by a similar change in another (to preserve the total). However, in order to ascertain the nature of this compensation it is important to understand how direct, individual perturbations affect the detector response.

The modular nature of the MCNP-PoliMi code system makes it possible to evaluate the partial responses for each reaction. Each reaction type may be processed individually to obtain the partial detector response. These partial responses may then be perturbed and combined, according to Eq. (5), to generate the total perturbed response.

2.3. MCNP-PoliMi model description

A range of monoenergetic photon sources were simulated to selectively explore the sensitivity of the photonuclear cross sections the entire resonance region (this is the region of greatest discrepancy observed in the literature). Sources of 8-, 9-, 10-, 11-, 12-, 13-, 14-, 15-, 16-, 17-, and 18-MeV photons were simulated with a 10-kg HEU target 1 m from a 50-by-50-cm^2, lead-shielded liquid scintillation detector. This system, shown in Fig. 3, is representative of current active interrogation systems under investigation for non-proliferation and homeland security applications. The gamma-ray energy range is the region where the greatest cross section discrepancies appear in the literature (Giacri-Mauborgne et al., 2006).

The MCNP-PoliMi detection post-processor was used to predict the TOF spectrum recorded by the liquid scintillation detector. The post-processing code uses the energy deposited in each particle collision (recorded by MCNP-PoliMi) and converts it into light produced by the scintillator. The total light generated by each particle track is computed and compared to a user-defined detection threshold. If the total light created during the pulse generation

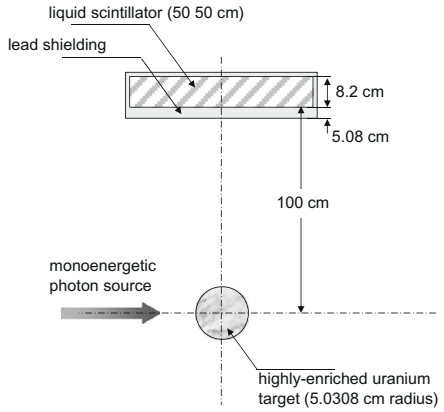

Fig. 3. MCNP-PoliMi model including the interrogation source, HEU target, and liquid scintillation detector.

time is greater than the threshold, one count is recorded at a specific time. The time difference between consecutive counts is compared to the deadtime defined by the user. A detection threshold of 0.0793 MeVee was applied in these simulations (this corresponds to the amount of light generated by a neutron depositing 500-keV). The deadtime was set to a typical value of 80 ns.

3. Perturbation results

Photoneutron production was analyzed with (γ,n), $(\gamma,2n)$, and (γ,f) cross section perturbations of −0.05, −0.10, −0.15, and −0.20 for each monoenergetic photon source. Fig. 4 shows the TOF count distribution from the 14-MeV beam using the unperturbed ENDF/B-VII cross sections. At this energy the (γ,n) and $(\gamma,2n)$ cross sections are equal, and much less than the (γ,f) cross section.

The small, initial peaks (at times less than 20 ns) are generated by the arrival of gamma-rays from photonuclear interactions in the target. This peak is relatively narrow since all gamma-rays travel at the same speed, and therefore arrive within a very short time window. The photoneutrons begin arriving at the detector at approximately 30 ns. In general, neutrons from $(\gamma,2n)$ reactions arrive later than other neutrons because they have a lower average energy. The widths of the neutron peaks are much greater than the gamma-ray

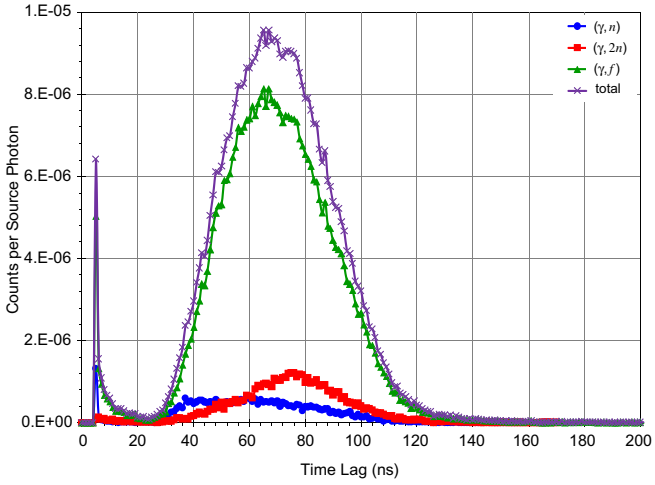

Fig. 4. Simulated TOF spectrum generated with a 14-MeV photon beam and a 0.0793 MeVee detection threshold; contributions from (γ,n), $(\gamma,2n)$, and (γ,f) reactions are shown.

Table 1
Integral photoneutron production (per source photon) using the unperturbed ENDF/B-VII cross sections.

E_γ (MeV)	Detected neutrons	Relative error
8	3.4617E-05	0.0034
9	3.4901E-05	0.0048
10	8.0934E-05	0.0052
11	1.3808E-04	0.0045
12	1.5523E-04	0.0046
13	1.7631E-04	0.0048
14	4.6497E-04	0.0029
15	1.7298E-04	0.0048
16	1.2218E-04	0.0048
17	1.9100E-04	0.0032
18	1.5683E-04	0.0033

peak because the neutrons have a distribution of velocities. The partial reaction contributions used to generate the perturbed response are also shown.

The neutron counts were integrated from 25 to 150 ns. This integration range was held constant for all perturbation cases and for all photon energies. The statistical error in the integrated values is proportional to the number of counts because of the analog nature of the MCNP simulations. Table 1 summarizes these results. The trend in these results follows the shape of the total cross section in Fig. 1. Because small perturbations do not change the total counts by a large amount, these statistical errors are approximately constant for all of the perturbed cases at each specific energy.

The change in the detector response relative to the base case for each perturbation, δ_n, was calculated by computing the variation in the detection rate due to each cross section variation

$$\Delta R_i = R_i^* - R_i, \tag{6}$$

and the relative variation in the detection rate due to the cross section variation

$$\delta n_i = \frac{\Delta R_i}{R_i}. \tag{7}$$

The relative variation of the number of detected neutrons at each photon energy is summarized in Tables 2–12. In Tables 7–12 there

Table 2
Relative change in detected neutrons produced by 8-MeV photons under (γ,n) and (γ,f) perturbations.

$\delta_{(\gamma,f)}$	$\delta_{(\gamma,n)}$				
	0.00	−0.50	−0.10	−0.15	−0.20
0.00	0.0000	−0.0193	−0.0385	−0.0578	−0.0770
−0.50	−0.0307	−0.0500	−0.0693	−0.0885	−0.1078
−0.10	−0.0615	−0.0807	−0.1000	−0.1193	−0.1385
−0.15	−0.0922	−0.1115	−0.1307	−0.1500	−0.1693
−0.20	−0.1230	−0.1422	−0.1615	−0.1807	−0.2000

Table 3
Relative change in detected neutrons produced by 9-MeV photons under (γ,n) and (γ,f) perturbations.

$\delta_{(\gamma,f)}$	$\delta_{(\gamma,n)}$				
	0.00	−0.50	−0.10	−0.15	−0.20
0.00	0.0000	−0.0149	−0.0297	−0.0446	−0.0595
−0.50	−0.0351	−0.0500	−0.0649	−0.0797	−0.0946
−0.10	−0.0703	−0.0851	−0.1000	−0.1149	−0.1297
−0.15	−0.1054	−0.1203	−0.1351	−0.1500	−0.1649
−0.20	−0.1405	−0.1554	−0.1703	−0.1851	−0.2000

Table 4
Relative change in detected neutrons produced by 10-MeV photons under (γ,n) and (γ,f) perturbations.

$\delta_{(\gamma,f)}$	$\delta_{(\gamma,n)}$				
	0.00	−0.50	−0.10	−0.15	−0.20
0.00	0.0000	−0.0148	−0.0295	−0.0443	−0.0591
−0.50	−0.0352	−0.0500	−0.0648	−0.0795	−0.0943
−0.10	−0.0705	−0.0852	−0.1000	−0.1148	−0.1295
−0.15	−0.1057	−0.1205	−0.1352	−0.1500	−0.1648
−0.20	−0.1409	−0.1557	−0.1705	−0.1852	−0.2000

Table 5
Relative change in detected neutrons produced by 11-MeV photons under (γ,n) and (γ,f) perturbations.

$\delta_{(\gamma,f)}$	$\delta_{(\gamma,n)}$				
	0.00	−0.50	−0.10	−0.15	−0.20
0.00	0.0000	−0.0158	−0.0317	−0.0475	−0.0633
−0.50	−0.0342	−0.0500	−0.0658	−0.0817	−0.0975
−0.10	−0.0683	−0.0842	−0.1000	−0.1158	−0.1317
−0.15	−0.1025	−0.1184	−0.1342	−0.1500	−0.1658
−0.20	−0.1367	−0.1525	−0.1684	−0.1842	−0.2000

Table 6
Relative change in detected neutrons produced by 12-MeV photons under (γ,n) and (γ,f) perturbations.

$\delta_{(\gamma,f)}$	$\delta_{(\gamma,n)}$				
	0.00	−0.50	−0.10	−0.15	−0.20
0.00	0.0000	−0.0118	−0.0236	−0.0353	−0.0471
−0.50	−0.0382	−0.0500	−0.0618	−0.0736	−0.0853
−0.10	−0.0764	−0.0882	−0.1000	−0.1118	−0.1236
−0.15	−0.1147	−0.1265	−0.1382	−0.1500	−0.1618
−0.20	−0.1529	−0.1647	−0.1765	−0.1882	−0.2000

Table 7
Relative change in detected neutrons produced by 13-MeV photons under (γ,n), $(\gamma,2n)$, and (γ,f) perturbations.

$\delta_{(\gamma,2n)}$	$\delta_{(\gamma,n)}$				
	0.00	−0.50	−0.10	−0.15	−0.20
0.00	0.0000	−0.0065	−0.0131	−0.0196	−0.0261
	−0.0417	−0.0482	−0.0548	−0.0613	−0.0678
	−0.0834	−0.0900	−0.0965	−0.1030	−0.1095
	−0.1251	−0.1317	−0.1382	−0.1447	−0.1513
	−0.1669	−0.1734	−0.1799	−0.1864	−0.1930
−0.50	−0.0018	−0.0083	−0.0148	−0.0213	−0.0279
	−0.0435	−0.0500	−0.0565	−0.0631	−0.0696
	−0.0852	−0.0917	−0.0982	−0.1048	−0.1113
	−0.1269	−0.1334	−0.1400	−0.1465	−0.1530
	−0.1686	−0.1751	−0.1817	−0.1882	−0.1947
−0.10	−0.0035	−0.0100	−0.0166	−0.0231	−0.0296
	−0.0452	−0.0518	−0.0583	−0.0648	−0.0713
	−0.0869	−0.0935	−0.1000	−0.1065	−0.1131
	−0.1287	−0.1352	−0.1417	−0.1482	−0.1548
	−0.1704	−0.1769	−0.1834	−0.1900	−0.1965
−0.15	−0.0053	−0.0118	−0.0183	−0.0249	−0.0314
	−0.0470	−0.0535	−0.0600	−0.0666	−0.0731
	−0.0887	−0.0952	−0.1018	−0.1083	−0.1148
	−0.1304	−0.1370	−0.1435	−0.1500	−0.1565
	−0.1721	−0.1787	−0.1852	−0.1917	−0.1982
−0.20	−0.0070	−0.0136	−0.0201	−0.0266	−0.0331
	−0.0487	−0.0553	−0.0618	−0.0683	−0.0749
	−0.0905	−0.0970	−0.1035	−0.1100	−0.1166
	−0.1322	−0.1387	−0.1452	−0.1518	−0.1583
	−0.1739	−0.1804	−0.1870	−0.1935	−0.2000

Table 8
Relative change in detected neutrons produced by 14-MeV photons under (γ,n), $(\gamma,2n)$, and (γ,f) perturbations.

$\delta_{(\gamma,2n)}$	$\delta_{(\gamma,n)}$				
	0.00	−0.50	−0.10	−0.15	−0.20
0.00	0.0000	−0.0033	−0.0065	−0.0098	−0.0130
	−0.0416	−0.0448	−0.0481	−0.0514	−0.0546
	−0.0832	−0.0864	−0.0897	−0.0929	−0.0962
	−0.1247	−0.1280	−0.1312	−0.1345	−0.1378
	−0.1663	−0.1696	−0.1728	−0.1761	−0.1793
−0.50	−0.0052	−0.0084	−0.0117	−0.0149	−0.0182
	−0.0467	−0.0500	−0.0533	−0.0565	−0.0598
	−0.0883	−0.0916	−0.0948	−0.0981	−0.1014
	−0.1299	−0.1332	−0.1364	−0.1397	−0.1429
	−0.1715	−0.1747	−0.1780	−0.1812	−0.1845
−0.10	−0.0103	−0.0136	−0.0168	−0.0201	−0.0234
	−0.0519	−0.0552	−0.0584	−0.0617	−0.0649
	−0.0935	−0.0967	−0.1000	−0.1033	−0.1065
	−0.1351	−0.1383	−0.1416	−0.1448	−0.1481
	−0.1766	−0.1799	−0.1832	−0.1864	−0.1897
−0.15	−0.0155	−0.0188	−0.0220	−0.0253	−0.0285
	−0.0571	−0.0603	−0.0636	−0.0668	−0.0701
	−0.0987	−0.1019	−0.1052	−0.1084	−0.1117
	−0.1402	−0.1435	−0.1467	−0.1500	−0.1533
	−0.1818	−0.1851	−0.1883	−0.1916	−0.1948
−0.20	−0.0207	−0.0239	−0.0272	−0.0304	−0.0337
	−0.0622	−0.0655	−0.0688	−0.0720	−0.0753
	−0.1038	−0.1071	−0.1103	−0.1136	−0.1169
	−0.1454	−0.1487	−0.1519	−0.1552	−0.1584
	−0.1870	−0.1902	−0.1935	−0.1967	−0.2000

Table 9
Relative change in detected neutrons produced by 15-MeV photons under (γ,n), $(\gamma,2n)$, and (γ,f) perturbations.

$\delta_{(\gamma,2n)}$	$\delta_{(\gamma,n)}$				
	0.00	−0.50	−0.10	−0.15	−0.20
0.00	0.0000	−0.0035	−0.0070	−0.0105	−0.0140
	−0.0413	−0.0448	−0.0483	−0.0518	−0.0553
	−0.0827	−0.0862	−0.0897	−0.0931	−0.0966
	−0.1240	−0.1275	−0.1310	−0.1345	−0.1380
	−0.1653	−0.1688	−0.1723	−0.1758	−0.1793
−0.50	−0.0052	−0.0087	−0.0122	−0.0157	−0.0191
	−0.0465	−0.0500	−0.0535	−0.0570	−0.0605
	−0.0878	−0.0913	−0.0948	−0.0983	−0.1018
	−0.1292	−0.1327	−0.1362	−0.1397	−0.1432
	−0.1705	−0.1740	−0.1775	−0.1810	−0.1845
−0.10	−0.0103	−0.0138	−0.0173	−0.0208	−0.0243
	−0.0517	−0.0552	−0.0587	−0.0622	−0.0657
	−0.0930	−0.0965	−0.1000	−0.1035	−0.1070
	−0.1344	−0.1378	−0.1413	−0.1448	−0.1483
	−0.1757	−0.1792	−0.1827	−0.1862	−0.1897
−0.15	−0.0155	−0.0190	−0.0225	−0.0260	−0.0295
	−0.0569	−0.0603	−0.0638	−0.0673	−0.0708
	−0.0982	−0.1017	−0.1052	−0.1087	−0.1122
	−0.1395	−0.1430	−0.1465	−0.1500	−0.1535
	−0.1809	−0.1844	−0.1878	−0.1913	−0.1948
−0.20	−0.0207	−0.0242	−0.0277	−0.0312	−0.0347
	−0.0620	−0.0655	−0.0690	−0.0725	−0.0760
	−0.1034	−0.1069	−0.1104	−0.1138	−0.1173
	−0.1447	−0.1482	−0.1517	−0.1552	−0.1587
	−0.1860	−0.1895	−0.1930	−0.1965	−0.2000

are five values listed for each (γ,n) and $(\gamma,2n)$ perturbation pair; these values correspond to (γ,f) perturbations of 0.0, −0.05, −0.10, −0.15, and −0.20.

It is clear from the results in Tables 2–12 that over the entire energy range perturbations in the (γ,f) cross section have the greatest

Table 10
Relative change in detected neutrons produced by 16-MeV photons under (γ,n), $(\gamma,2n)$, and (γ,f) perturbations.

$\delta_{(\gamma,2n)}$	$\delta_{(\gamma,n)}$				
	0.00	−0.50	−0.10	−0.15	−0.20
0.00	0.0000	−0.0026	−0.0052	−0.0078	−0.0103
	−0.0422	−0.0448	−0.0473	−0.0499	−0.0525
	−0.0843	−0.0869	−0.0895	−0.0921	−0.0947
	−0.1265	−0.1291	−0.1317	−0.1343	−0.1369
	−0.1687	−0.1713	−0.1739	−0.1764	−0.1790
−0.50	−0.0052	−0.0078	−0.0104	−0.0130	−0.0156
	−0.0474	−0.0500	−0.0526	−0.0552	−0.0578
	−0.0896	−0.0922	−0.0948	−0.0973	−0.0999
	−0.1318	−0.1343	−0.1369	−0.1395	−0.1421
	−0.1739	−0.1765	−0.1791	−0.1817	−0.1843
−0.10	−0.0105	−0.0131	−0.0157	−0.0182	−0.0208
	−0.0527	−0.0552	−0.0578	−0.0604	−0.0630
	−0.0948	−0.0974	−0.1000	−0.1026	−0.1052
	−0.1370	−0.1396	−0.1422	−0.1448	−0.1473
	−0.1792	−0.1818	−0.1843	−0.1869	−0.1895
−0.15	−0.0157	−0.0183	−0.0209	−0.0235	−0.0261
	−0.0579	−0.0605	−0.0631	−0.0657	−0.0682
	−0.1001	−0.1027	−0.1052	−0.1078	−0.1104
	−0.1422	−0.1448	−0.1474	−0.1500	−0.1526
	−0.1844	−0.1870	−0.1896	−0.1922	−0.1948
−0.20	−0.0210	−0.0236	−0.0261	−0.0287	−0.0313
	−0.0631	−0.0657	−0.0683	−0.0709	−0.0735
	−0.1053	−0.1079	−0.1105	−0.1131	−0.1157
	−0.1475	−0.1501	−0.1527	−0.1552	−0.1578
	−0.1897	−0.1922	−0.1948	−0.1974	−0.2000

Table 11
Relative change in detected neutrons produced by 17-MeV photons under (γ,n), $(\gamma,2n)$, and (γ,f) perturbations.

$\delta_{(\gamma,2n)}$	$\delta_{(\gamma,n)}$				
	0.00	−0.50	−0.10	−0.15	−0.20
0.00	0.0000	−0.0018	−0.0035	−0.0053	−0.0071
	−0.0458	−0.0475	−0.0493	−0.0511	−0.0528
	−0.0915	−0.0933	−0.0951	−0.0968	−0.0986
	−0.1373	−0.1391	−0.1408	−0.1426	−0.1444
	−0.1831	−0.1848	−0.1866	−0.1884	−0.1901
−0.50	−0.0025	−0.0042	−0.0060	−0.0078	−0.0096
	−0.0482	−0.0500	−0.0518	−0.0535	−0.0553
	−0.0940	−0.0958	−0.0975	−0.0993	−0.1011
	−0.1398	−0.1415	−0.1433	−0.1451	−0.1468
	−0.1855	−0.1873	−0.1891	−0.1908	−0.1926
−0.10	−0.0049	−0.0067	−0.0085	−0.0102	−0.0120
	−0.0507	−0.0525	−0.0542	−0.0560	−0.0578
	−0.0965	−0.0982	−0.1000	−0.1018	−0.1035
	−0.1422	−0.1440	−0.1458	−0.1475	−0.1493
	−0.1880	−0.1898	−0.1915	−0.1933	−0.1951
−0.15	−0.0074	−0.0092	−0.0109	−0.0127	−0.0145
	−0.0532	−0.0549	−0.0567	−0.0585	−0.0602
	−0.0989	−0.1007	−0.1025	−0.1042	−0.1060
	−0.1447	−0.1465	−0.1482	−0.1500	−0.1518
	−0.1905	−0.1922	−0.1940	−0.1958	−0.1975
−0.20	−0.0099	−0.0116	−0.0134	−0.0152	−0.0170
	−0.0556	−0.0574	−0.0592	−0.0609	−0.0627
	−0.1014	−0.1032	−0.1049	−0.1067	−0.1085
	−0.1472	−0.1489	−0.1507	−0.1525	−0.1542
	−0.1929	−0.1947	−0.1965	−0.1982	−0.2000

influence on the number of detected neutrons. This is even true for photon energies from 9 to 12 MeV where the (γ,n) cross section is greater than the (γ,f) cross section. This is due primarily to the multiplicity of the fission reaction: on average, each fission reaction releases 2–3 neutrons. It should be noted that the multiplicity

Table 12
Relative change in detected neutrons produced by 18-MeV photons under (γ,n), $(\gamma,2n)$, and (γ,f) perturbations.

$\delta_{(\gamma,2n)}$	$\delta_{(\gamma,n)}$				
	0.00	−0.50	−0.10	−0.15	−0.20
0.00	0.0000	−0.0019	−0.0037	−0.0056	−0.0075
	−0.0468	−0.0487	−0.0506	−0.0525	−0.0543
	−0.0937	−0.0955	−0.0974	−0.0993	−0.1012
	−0.1405	−0.1424	−0.1443	−0.1461	−0.1480
	−0.1873	−0.1892	−0.1911	−0.1930	−0.1948
−0.50	−0.0013	−0.0032	−0.0050	−0.0069	−0.0088
	−0.0481	−0.0500	−0.0519	−0.0537	−0.0556
	−0.0950	−0.0968	−0.0987	−0.1006	−0.1025
	−0.1418	−0.1437	−0.1455	−0.1474	−0.1493
	−0.1886	−0.1905	−0.1924	−0.1943	−0.1961
−0.10	−0.0026	−0.0045	−0.0063	−0.0082	−0.0101
	−0.0494	−0.0513	−0.0532	−0.0550	−0.0569
	−0.0963	−0.0981	−0.1000	−0.1019	−0.1037
	−0.1431	−0.1450	−0.1468	−0.1487	−0.1506
	−0.1899	−0.1918	−0.1937	−0.1955	−0.1974
−0.15	−0.0039	−0.0058	−0.0076	−0.0095	−0.0114
	−0.0507	−0.0526	−0.0545	−0.0563	−0.0582
	−0.0976	−0.0994	−0.1013	−0.1032	−0.1050
	−0.1444	−0.1463	−0.1481	−0.1500	−0.1519
	−0.1912	−0.1931	−0.1950	−0.1968	−0.1987
−0.20	−0.0052	−0.0070	−0.0089	−0.0108	−0.0127
	−0.0520	−0.0539	−0.0558	−0.0576	−0.0595
	−0.0988	−0.1007	−0.1026	−0.1045	−0.1063
	−0.1457	−0.1476	−0.1494	−0.1513	−0.1532
	−0.1925	−0.1944	−0.1963	−0.1981	−0.2000

Table 13
Photoneutron production sensitivity with respect to perturbations in the (γ,n), $(\gamma,2n)$, and (γ,f) reaction cross sections (denoted S_1, S_2, and S_3, respectively).

E_γ (MeV)	S_1	S_2	S_3
8	0.3852	0.0000	0.6149
9	0.3042	0.0000	0.6958
10	0.3241	0.0000	0.6759
11	0.3295	0.0000	0.6705
12	0.2355	0.0000	0.7645
13	0.1148	0.0388	0.8465
14	0.0652	0.1033	0.8315
15	0.0580	0.1134	0.8286
16	0.0434	0.1049	0.8517
17	0.0354	0.0493	0.9153
18	0.0374	0.0259	0.9367

of the HEU sample is not a factor in these results because it is a constant factor of the material.

The sensitivity coefficients for photoneutron detection were computed by dividing the relative change in Eq. (7) by the relative magnitude of the cross section perturbation δ_i with the other cross sections being held constant

$$S_i = \left.\frac{\delta n_i}{\delta_i}\right|_{\delta_{j\neq i}=0}. \tag{8}$$

Table 13 lists the S_1, S_2, and S_3 values for perturbations in the (γ,n), $(\gamma,2n)$, and (γ,f) cross sections, respectively. Photon energies less than 13-MeV are below the threshold of a $(\gamma,2n)$ reaction (E_{th} = 12.14 MeV), therefore, perturbations to the $(\gamma,2n)$ cross section have no effect.

Fig. 5 shows the sensitivity results plotted as a function of gamma-ray energy. At relatively low energies (E_γ < 12 MeV), the number of detected neutrons is approximately 70% sensitive to changes in the (γ,f) cross section and 30% sensitive to changes in the (γ,n) cross section. As gamma-ray energy increases the (γ,f) sensitivity

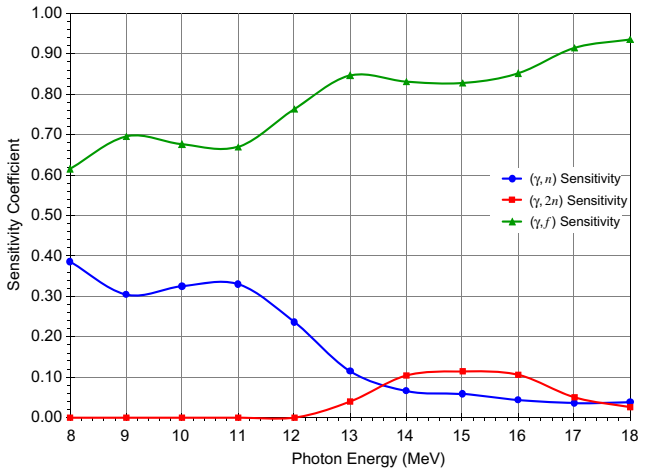

Fig. 5. Photoneutron detection sensitivity to perturbations in (γ,n), $(\gamma,2n)$, and (γ,f) cross sections as a function of photon energy.

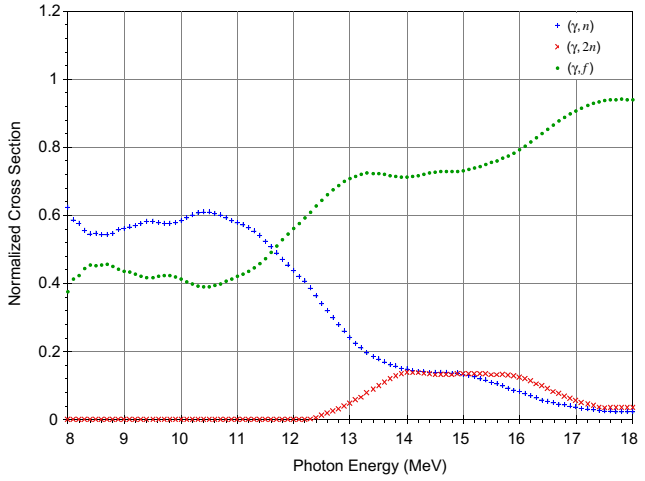

Fig. 6. Normalized photonuclear reaction cross sections in the energy region of interest for ^{235}U.

increases and the (γ,n) sensitivity decreases. There is a small (approximately 10%) sensitivity to $(\gamma,2n)$ perturbations in the energy range between 15 and 17 MeV.

Fig. 6 shows the normalized photonuclear cross sections for gamma-ray energies between 8 and 18 MeV. It is clear that the sensitivity response at any given gamma-ray energy depends directly on the relative magnitude of the photonuclear cross sections.

Gamma-rays with energies in the range of 9–20 MeV are favored for currently-proposed active interrogation technologies. In this energy region the ability of modern simulation tools to predict the photonuclear response is greatly limited due to the high sensitivity of the simulated results to observed discrepancies in photonuclear cross section data.

4. Conclusions

The sensitivity of the photoneutron production in DU to perturbations in the (γ,n), $(\gamma,2n)$, and (γ,f) cross sections of ^{235}U has been investigated using the MCNPX/MCNP-PoliMi code system. The analysis was performed using a new methodology that utilizes the modular nature of this code system to provide a fast and efficient method for analyzing the sensitivity of detector response to photonuclear cross section perturbations.

The results indicate that the photoneutron production at relatively low energies (E_γ < 12 MeV), the number of detected neutrons is approximately 70% sensitive to changes in the (γ,f) cross section and 30% sensitive to changes in the (γ,n) cross section. As gamma-ray energy increases the (γ,f) sensitivity increases and the (γ,n) sensitivity decreases. There is a small (approximately 10%) sensitivity to $(\gamma,2n)$ perturbations in the energy range between 15 and 17 MeV. These trends are consistent with those observed in the normalized reaction cross sections of ^{235}U.

These specific results apply only to the source–target configuration considered here. However, the methodology is general and may be readily applied to any source–target configuration to assess the effects of photonuclear cross section perturbations on the simulated detector response. In the future other cross section libraries will also be explored (e.g. JEFF or JENDL).

References

Caldwell, J.T. et al., 1980. Giant resonance for actinide nuclei: photoneutron and photofission cross sections of ^{235}U, ^{236}U, ^{238}U and ^{232}Th. Phys. Rev. C 21 (4), 1215–1231.

Clarke, S. et al., 2008. Sensitivity of photoneutron production to perturbations in cross-section data. Nucl. Sci. Eng. 160 (3), 370–377.

Dupont, E., et al. 2007. Photonuclear data evaluations of actinides up to 130 MeV. In: Proceedings of the International Conference on Nuclear Data for Science and Technology (ND2007), April 21–27, Nice, France.

Flaska, M. et al., 2004. Modeling of the GELINA neutron target using coupled electron–photon–neutron transport with the MCNP4C3 code. Nucl. Intrum. Meth. A 531 (4), 392–406.

Giacri-Mauborgne, M.-L. et al., 2006. Photonuclear physics in radiation transport-III: actinide cross sections and spectra. Nucl. Sci. Eng. 153, 33–40.

Pelowitz, D. (Ed.), 2005. MCNPX User's Manual, Version 2.5.0. Los Alamos National Laboratory, LA-CP-05-0369.

Pozzi, S., et al. 2007. MCNP-PoliMi Post-Processing Code Ver. 1.9. Oak Ridge National Laboratory Internal Report, ORNL/TM-2007/33.

Varmalov, A.V., et al. 1999. Atlas of Giant Dipole Resonance Parameters and Graphs of Photonuclear Reaction Cross Sections. INDC(NDS)-399, International Atomic Energy Agency, International Nuclear Data Committee.